Chinese Chemical Letters 31 (2020) 2037–2040

Contents lists available at ScienceDirect

Chinese Chemical Letters

journal homepage: www.elsevier.com/locate/cclet

Communication

Synthesis and *in-situ* noble metal modification of $WO_3 \cdot 0.33H_2O$ nanorods from a tungsten-containing mineral for enhancing NH_3 sensing performance

Tingting Li[a], Yanbai Shen[a,c,*], Sikai Zhao[a], Pengfei Zhou[a], Xiangxi Zhong[a], Shuling Gao[a,*], Dezhou Wei[a], Fanli Meng[b]

[a] School of Resources and Civil Engineering, Northeastern University, Shenyang 110819, China
[b] School of Information Science and Engineering, Northeastern University, Shenyang 110819, China
[c] State Environmental Protection Key Laboratory of Mineral Metallurgical Resources Utilization and Pollution Control, Wuhan University of Science and Technology, Wuhan 430081, China

ARTICLE INFO

Article history:
Received 19 December 2019
Received in revised form 7 January 2020
Accepted 9 January 2020
Available online 9 January 2020

Keywords:
Scheelite concentrate
Noble metal doping
$WO_3 \cdot 0.33H_2O$ nanorods
NH_3
Sensing mechanism

ABSTRACT

Ag- and Pt-doped $WO_3 \cdot 0.33H_2O$ nanorods with high response and selectivity to NH_3 were synthesized from a tungsten-containing mineral of scheelite concentrate by a simple combined process, namely by a high pressure leaching method to obtain tungstate ions-containing leaching solution and followed by a hydrothermal method to prepare corresponding nanorods. The microstructure and NH_3 sensing performance of the final products were investigated systematically. The microstructure characterization showed that the as-prepared $WO_3 \cdot 0.33H_2O$ nanorods had a hexagonal crystal structure, and Ag and Pt nanoparticles were uniformly distributed in the $WO_3 \cdot 0.33H_2O$ nanorods. Gas sensing measurements indicated that Ag and Pt nanoparticles not only could obviously enhance NH_3 sensing properties in terms of response, selectivity as well as response/recovery time, but also could reduce the optimal operating temperature at which the highest response was achieved. The highest responses of 22.4 and 47.6 for Ag- and Pt-doped $WO_3 \cdot 0.33H_2O$ nanorods to 1000 ppm NH_3 were obtained at 225 and 175 °C, respectively, which were about four and eight folds higher than that of pure one at 250 °C. The superior NH_3 sensing properties are mainly ascribed to the catalytic activities of noble metals and the different work functions between noble metals and $WO_3 \cdot 0.33H_2O$.

Over the past decade years, a lot of attempts have been made to prepare $WO_3 \cdot \chi H_2O$ sensing materials with the enhancement of sensitivity, response/recovery speed, long-term stability as well as selectivity [1]. As actively catalytic dopants, noble metals have been frequently used to modify the surface properties and electronic structure of the sensing material to improve the gas sensing properties due to their excellent sensitization effects as well as the improvement in the chemical and thermal stability of the active layer, which can change the morphology and energy band structure of a metal-oxide-semiconductor (MOS) material and correspondingly cause an increase in the center of gas reaction on the sensing material surface [2–8].

As a typical gas sensing material with good application prospects, $WO_3 \cdot \chi H_2O$ presents excellent sensing performance. However, the practical application of $WO_3 \cdot \chi H_2O$ in gas sensor is relatively few, which is mainly affected by atmosphere humidity and raw material price. At present, the raw materials used for preparing $WO_3 \cdot \chi H_2O$ sensing materials are basically analytical reagents such as sodium tungstate, tungsten hexachloride and ammonium metatungstate, or some ultra-high purity tungsten metals. These raw materials from commercial sources are relatively expensive, and it also brings out some pollution in the preparation processes. Therefore, it is a very meaningful work to find a cheaper tungsten-containing raw material to synthesize $WO_3 \cdot \chi H_2O$ sensing materials.

Scheelite concentrate is the main material used for tungsten smelting. Usually, scheelite concentrate is often associated with some precious noble metals such as Pt, Au, Ag and Pd. Therefore, in the present work, a low-grade scheelite concentrate was selected as the raw material to prepare $WO_3 \cdot \chi H_2O$ sensing materials. Also,

* Corresponding authors at: School of Resources and Civil Engineering, Northeastern University, Shenyang 110819, China.
E-mail addresses: shenyanbai@mail.neu.edu.cn (Y. Shen), gaoshuling@mail.neu.edu.cn (S. Gao).

https://doi.org/10.1016/j.cclet.2020.01.024

to simulate the existence of some noble metals in scheelite concentrate, the effect of *in-situ* doping of noble metals on the $WO_3 \cdot \chi H_2O$ microstructure and its gas sensing properties were investigated systematically.

The whole preparation process of $WO_3 \cdot 0.33H_2O$ samples mainly involves two steps. One step is to convert calcium tungstate in scheelite concentrate into soluble tungstate salt by a leaching method with sodium hydroxide as the leaching reagent. The leaching solution can be obtained according to the previous references [9,10]. The as-obtained leaching solution mainly contains 122.2 g/L of W, 0.061 g/L of As, 0.52 g/L of Mo and 0.33 g/L of Si. The impurity contents in the leaching solution are less, which have little effect on the preparation of the subsequent samples.

The other step is to prepare pure, Ag- and Pt-doped $WO_3 \cdot 0.33H_2O$ nanorods by a simple hydrothermal method from soluble tungstate salt. As is well known, Na^+ ions can play an end-capping role in the preparation process of $WO_3 \cdot 0.33H_2O$ nanomaterials. In order to avoid the influence of large amounts of Na^+ ions introduced by sodium hydroxide (NaOH) leaching agent, 24 mL of 3 mol/L HCl solution was added to 10 mL of the above leaching solution to form white tungstic acid precipitate, which was subsequently treated by filtering and washing for several times with deionized water. Subsequently, the above precipitate was transferred to a 250 mL beaker by introducing 50 mL of deionized water, and then 0.27 g of NaOH were added to dissolve the tungstic acid precipitate under vigorous stirring until the precipitate was completely dissolved and the pH value of the as-obtained solution was about 7. Then, 1.5 g of NaCl was placed into the aforementioned dissolved solution and continuously stirred for 10 min. In order to prepare Ag- and Pt-doped $WO_3 \cdot 0.33H_2O$ nanorods, a certain amount of silver nitrate solution (1.699 g/L) or chloroplatinic acid solution (6.706 g/L) was put into the above-mentioned solution and vigorously stirred for 10 min, of which the molar ratio of Ag/W or Pt/W was determined to be 0.4 mol%. Then 3 mol/L of HCl solution was dropwise added into the above mixed solution until a mixed solution with the pH value of 2.2 was obtained. The mixed solution was continuously stirred for 10 min, and then transferred to a 100 mL Teflon-sealed autoclave and heated at 200 °C for 12 h. After the reaction, the as-prepared precipitant was transferred from the cooled autoclave into a beaker and treated by filtering and washing with deionized water, and then drying treatment was carried out at a drying oven. The dried products were annealed at 400 °C for 4 h in air to obtain a stable crystal structure. The structure characteristics of these samples were characterized by X-ray diffraction (XRD, PA Nalytical X'Pert Pro), field-emission scanning electron microscopy (FESEM, ZEISS Ultra Plus), high-resolution transmission electron microscopy (TEM, FEIG^2-20) and X-ray photoelectron spectroscopy (XPS, ESCALAB 250 Xi).

The sensor device was prepared according to the previous reference [9]. A static test system was adopted to evaluate the gas sensing performance of the as-prepared $WO_3 \cdot 0.33H_2O$ nanorods. For each type of gas sensor, three sensor samples were simultaneously tested in the gas sensing measurements. A specific concentration (10–1000 ppm) of NH_3 gas was prepared in a test chamber with a capacity of 18 L by evaporating a certain volume of ammonia water with a concentration of 25%–28%. The sensor response (S) was determined as $S = R_a/R_g$, where R_g and R_a were the sensor resistance in the detected gas and in air, respectively. The response and recovery times were defined according to the reference [9].

XRD patterns of the as-prepared pure, Ag- and Pt-doped products were presented in Fig. S1 (Supporting information). Obviously, all characteristic peaks of the three samples demonstrate a hexagonal phase of tungsten oxide hydrate of $WO_3 \cdot 0.33H_2O$ (JCPDS card No. 35-1001). The strong and narrow peaks of the three samples also reveal a good crystallinity. Obviously, the diffraction peaks of Ag-doped sample show relatively lower intensity compared with those of pure one, demonstrating that Ag doping restricts the growth of $WO_3 \cdot 0.33H_2O$ nanorods. However, the corresponding peaks of Pt-doped sample show higher intensity compared with those of pure one, revealing that Pt doping is beneficial to the growth of $WO_3 \cdot 0.33H_2O$ nanorods. Additionally, there are no other characteristic peaks of impurities, revealing that the three $WO_3 \cdot 0.33H_2O$ samples have high purity. Meanwhile, the peaks correlated to Ag or Pt are not found, which may be attributed to the low content of Ag or Pt in $WO_3 \cdot 0.33H_2O$ sample.

Fig. 1 illustrates low- and high-magnification SEM images of pure, Ag-, and Pt-doped $WO_3 \cdot 0.33H_2O$ nanorods. The pure nanorods are less than 5 μm in length and 100–200 nm in diameter, showing a fairly uniform shape. Ag-doped $WO_3 \cdot 0.33H_2O$ with a rough and dense surface is mainly composed of shorter nanorods which are less than 4.5 μm in length and 100–400 nm in diameter, revealing that Ag doping results in the growth of nanorods in a denser and shorter direction. However, Pt-doped $WO_3 \cdot 0.33H_2O$ is mainly composed of longer nanorods which are approximately 10 μm in length and 100–500 nm in diameter, indicating that Pt doping is beneficial to the growth of nanorods in a longer and thicker direction. Additionally, many finer nanoribbons with the width of 20–50 nm peel off from the surface of Pt-doped $WO_3 \cdot 0.33H_2O$ nanorods, revealing that the nanorods are self-assembled by numerous finer nanoribbons in the same direction, which is conducive to increasing the specific surface area and surface defects of the products, and correspondingly enhancing the gas sensing properties. The length-to-diameter ratios of pure, Ag- and Pt-doped nanorods are appropriately 12.2, 6.1 and 24.4, respectively, which is consistent with the XRD results.

The surface morphology and crystal structure of noble metal-modified $WO_3 \cdot 0.33H_2O$ nanorods were further examined by TEM technique, as presented in Fig. S2 (Supporting information). As shown in Figs. S2a and c, the single Ag-doped nanorod has a smooth surface, and the Pt-doped nanorod shows a coarse surface

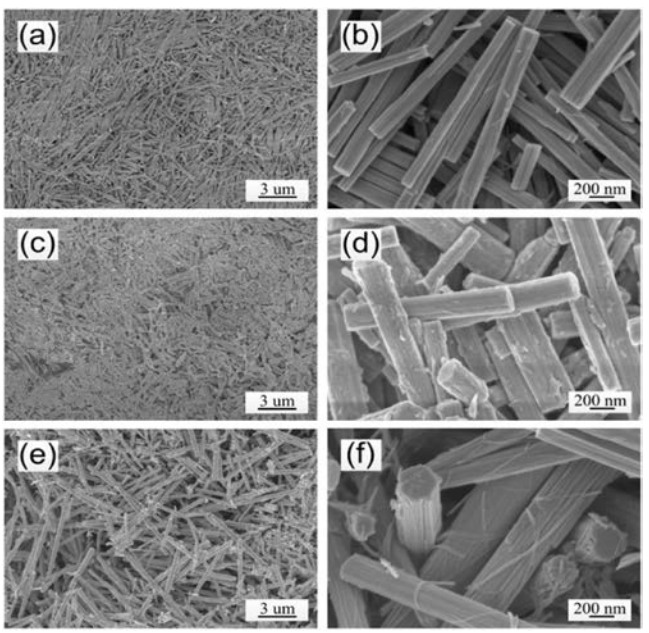

Fig. 1. Low-magnification SEM images of (a) pure, (c) Ag- and (e) Pt-doped $WO_3 \cdot 0.33H_2O$ nanorods. High-magnification SEM images of (b) pure, (d) Ag- and (f) Pt-doped $WO_3 \cdot 0.33H_2O$ nanorods.

at which some finer nanoribbons occur. The interplanar spacing of 0.365 nm in Figs. S2b and d is in accordance with the (110) crystal plane of the hexagonal $WO_3{\cdot}0.33H_2O$. The interplanar spacings of 0.236 and 0.279 nm in Fig. S2b are in agreement with the (111) crystal plane of Ag and the (200) crystal plane of Ag_2O, respectively. Also, the interplanar spacings of 0.196 and 0.319 nm in Fig. S2d correspond to the (200) crystal plane of Pt and the (110) crystal plane of PtO_2. It demonstrates that Ag and Pt are partially oxidized in final products in the annealing process.

Fig. S3 (Supporting information) shows the elemental distribution states of Ag- and Pt-doped $WO_3{\cdot}0.33H_2O$ nanorods. It is found that the noble metal-doped $WO_3{\cdot}0.33H_2O$ nanorods are composed of W, O, and corresponding noble metal. Ag and Pt elements are homogenously distributed in nanorods in the form of nanoparticles. Because the noble metals have a higher electrical conductivity compared with $WO_3{\cdot}0.33H_2O$, it is beneficial to accelerate electron transfer and simultaneously catalyze the chemical reactions between the detected gas molecules and the chemical adsorbed oxygen ions in $WO_3{\cdot}0.33H_2O$ [11]. Additionally, the uniform distribution of noble metal nanoparticles in $WO_3{\cdot}0.33H_2O$ can increase the adsorption sites in sensing layer, leading to the improvement of the sensor response [12]. Moreover, noble metals are *in-situ* doped in nanorods and Ag/Ag_2O or Pt/PtO_2 nanoparticles also exist in the interior of nanorods, which can increase the crystal defects of the sensing materials and correspondingly is conductive to the enhancement of sensing properties.

XPS spectra of Ag- and Pt-doped $WO_3{\cdot}0.33H_2O$ nanorods are shown in Fig. S4 (Supporting information) to evaluate their surface elemental composition and metallic state. The XPS survey scan reveals that O, W and corresponding noble metal elements are found on the surface layers of the as-prepared $WO_3{\cdot}0.33H_2O$ nanorods. The peaks at the binding energies of 530.48 eV (Fig. S4a) and 530.58 eV (Fig. S4d) correspond to O^{2-} ions of $WO_3{\cdot}0.33H_2O$, which belong to the lattice oxygen atoms [13,14]. The peaks at the binding energies of 35.88 and 37.98 eV (Figs. S4b and e) are ascribed to W $4f_{7/2}$ and W $4f_{5/2}$, respectively, revealing the existence of W^{6+} oxidation state in $WO_3{\cdot}0.33H_2O$ nanorods [15,16]. The singlet peak centred at the binding energy of 41.58 eV (Figs. S4b and e) is contributed to W $5p_{3/2}$ [17]. The peaks located at the binding energies of 368.08 and 373.58 eV in Fig. S4c correspond to Ag $3d_{5/2}$ and Ag $3d_{3/2}$, respectively. These values reveal that Ag nanoparticles not only exist in the form of metallic Ag, but also present in the silver oxide (Ag_2O) form, demonstrating the partial oxidation of Ag nanoparticles and the co-existence of Ag and Ag_2O in $WO_3{\cdot}0.33H_2O$ [14,18]. The stronger peak in Fig. S4f at the binding energy of 79.28 eV is ascribed to Pt $4f_{5/2}$, indicating the formation of PtO_2, and the weaker peaks at 70.98 and 74.28 eV are assigned to Pt $4f_{7/2}$ and Pt $4f_{5/2}$, respectively, indicating that a small amount of the metallic Pt is formed [19,20].

Fig. 2a shows the responses of pure, Ag- and Pt-doped $WO_3{\cdot}0.33H_2O$ nanorods to 1000 ppm NH_3 at different operating temperatures. Obviously, except for the pure nanorods, the response curves of Ag- and Pt-doped nanorods exhibit a volcanic-shape at operating temperature ranging from 75 °C to 250 °C. It can be seen that the noble metal doping can obviously improve the sensor response and reduce the optimum operating temperature. Compared with pure and Ag-doped nanorods, the Pt-doped $WO_3{\cdot}0.33H_2O$ nanorods present the highest response and a relatively lower operating temperature. The highest responses of 22.4 and 47.6 for Ag- and Pt-doped nanorods can be achieved at 225 and 175 °C, respectively, which are about four and eight times higher than that of 5.8 for pure one at 250 °C. The results on the selectivity of the three samples to various types of detected gases at their optimum operating temperatures are shown in Fig. 2b. Notably, compared with pure nanorods, Ag- or Pt-doped nanorods exhibit more superior selectivity to NH_3. The responses of Ag-doped nanorods to 1000 ppm NH_3, 1000 ppm methanol, 100 ppm acetone, 100 ppm methylbenzene, 100 ppm SO_2 and 1000 ppm methanal at 225 °C are 22.4, 12.1, 4.9, 6.6, 8.4 and 12.0, respectively. The responses of Pt-doped nanorods towards the above detected gases at 175 °C are 47.6, 1.0, 1.4, 1.1, 1.6 and 1.1, respectively. Obviously, Pt-doped nanorods show more excellent selectivity to NH_3 in comparison with pure and Ag-doped nanorods, which may be attributed to the fact that the higher operating temperatures leads to better sensitivity to some volatile gases.

Figs. S5a and b (Supporting information) display the transient resistances of noble metal-doped $WO_3{\cdot}0.33H_2O$ nanorods to various concentrations of NH_3 in the range of 10–1000 ppm at their optimum operating temperatures. For each concentration of NH_3, the sensor resistance has a rapid decrease with the introduction of NH_3, followed by an increase with the release of NH_3, indicating that the as-synthesized $WO_3{\cdot}0.33H_2O$ nanorods are n-type MOS materials. For each sensor, the amplitude change in the resistance has a gradual increase along with the increase of NH_3 concentration. Figs. S5c and d (Supporting information) illustrate the transient resistances of the two sensors to 1000 ppm NH_3 at their optimum operating temperatures. Obviously, the response time of Pt-doped nanorods is shorter than that of Ag-doped one, and the recovery time of the former is longer than that of the latter, which is attributed to the various catalytic activities of Ag/Ag_2O and Pt/PtO_2. Compared with Ag/Ag_2O, Pt/PtO_2 have higher catalytic activity to NH_3, which are more beneficial to decrease the activation barrier as well as accelerate the dissociation of the N—H bond, therefore the response time is shorter [19]. However, because of the higher response of Pt-doped $WO_3{\cdot}0.33H_2O$ nanorods to NH_3, the recovery time is relatively longer.

Fig. 3 illustrates the long-term stability of Ag- and Pt-doped $WO_3{\cdot}0.33H_2O$ nanorods upon exposure to 1000 ppm NH_3 at their optimum operating temperatures during 30 days. As seen in this figure, there is no obvious decrease or increase in the sensor response, reflecting a good long-term stability of the as-synthesized Ag- and Pt-doped $WO_3{\cdot}0.33H_2O$ nanorods.

The improved gas sensing properties of $WO_3{\cdot}0.33H_2O$ nanorods modified with Ag and Pt can be ascribed to the catalytic activities of noble metals and the various work functions of noble metals and $WO_3{\cdot}0.33H_2O$ [21–24]. During the process of catalytic reaction, NH_3 molecules will be more easily chemisorbed and subsequently activated on the surfaces of noble metal nanoparticles, and eventually decomposed into the corresponding ions [25,26]. Then, the as-produced ions are transformed to $WO_3{\cdot}0.33H_2O$ surface, and react with the chemisorbed oxygen ions on the surface of the nanorods, thereby resulting in a decrease in the sensor resistance and subsequent an enhancement in the sensor response [12,27]. In addition, since the different work function energies of $WO_3{\cdot}0.33H_2O$ (5.7 eV), Ag/Ag_2O (4.26/5.0 eV) and Pt/PtO_2 (5.12/5.93 eV), this will result in the formation of heterojunction at their interface and free electron transfer until their Femi levels equalize, thereby causing a shrink in the depletion layer width of $WO_3{\cdot}0.33H_2O$, which is beneficial to the enhancement of gas sensing properties [28]. Additionally, the enhanced gas sensing properties of Ag-doped nanorods are not directly related to its length-to-diameter, and the improvement in sensing performance of Pt-doped nanorods may be partly attributed to their larger length-to-diameter.

In conclusion, Ag- and Pt-doped $WO_3{\cdot}0.33H_2O$ nanorods with high response and selectivity to NH_3 were successfully synthesized from a low-grade scheelite concentrate by a simple combined process, namely by a high-pressure leaching process, followed by a hydrothermal synthesis. $WO_3{\cdot}0.33H_2O$ nanorods with about 5 μm in length and 100–200 nm in diameter had a hexagonal crystal structure, and Ag and Pt nanoparticles were uniformly distributed

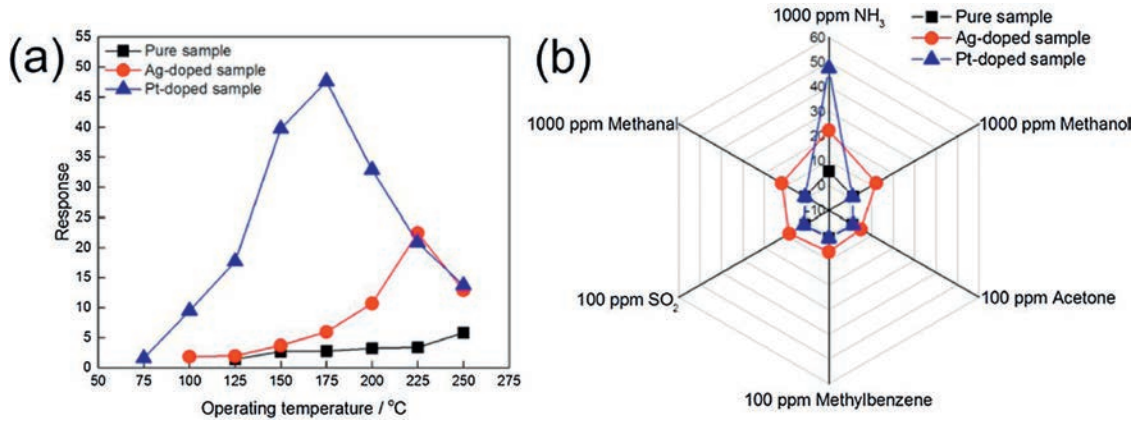

Fig. 2. (a) Responses *vs.* operating temperature of pure, Ag- and Pt-doped $WO_3 \cdot 0.33H_2O$ nanorods to 1000 ppm NH_3. (b) Selectivity of the three samples to various detected gases at their optimum operating temperatures.

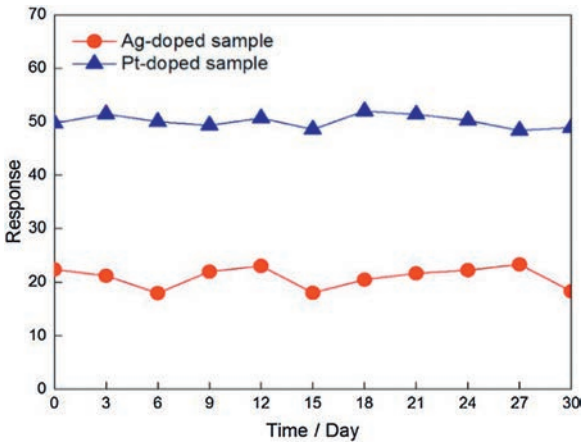

Fig. 3. Long-term stability of Ag-, and Pt-doped $WO_3 \cdot 0.33H_2O$ nanorods to 1000 ppm NH_3 at their optimum operating temperatures.

in $WO_3 \cdot 0.33H_2O$ nanorods. Noble metal-doped $WO_3 \cdot 0.33H_2O$ nanorods exhibited an obviously improved gas sensing properties in comparison with pure one, especially in the terms of response, selectivity, optimum operating temperature, and response/recovery speed. Especially, Pt-doped $WO_3 \cdot 0.33H_2O$ nanorods showed highest response, lowest optimum operating temperature, best selectivity to NH_3 and long-term stability. The enhancement in the sensing performance could be contributed to the various catalytic activities of noble metals and the different work functions of noble metals and $WO_3 \cdot 0.33H_2O$ nanorods.

Declaration of competing interest

The authors declare that they have no known competing financial interests or personal relationships that could have appeared to influence the work reported in this paper.

Acknowledgments

The project was supported by the National Natural Science Foundation of China (Nos. 51674067, 51422402), Fundamental Research Funds for the Central Universities (Nos. N180102032, N180106002, N180408018, N170106005), Liaoning Revitalization Talents Program (No. XLYC1807160), Liaoning BaiQianWan Talents Program (No. 201892127), Open Foundation of State Key Laboratory of Mineral Processing (No. BGRIMM-KJSKL-2019-12) and Open Foundation of State Environmental Protection Key Laboratory of Mineral Metallurgical Resources Utilization and Pollution Control (No. HB201902).

Appendix A. Supplementary data

Supplementary material related to this article can be found, in the online version, at doi:https://doi.org/10.1016/j.cclet.2020.01.024.

References

[1] F.P. Duanmu, Z.R. Shen, Q. Liu, et al., Chin. Chem. Lett. 31 (2020) 1114–1118.
[2] R.S. Ganesh, E. Durgadevi, M. Navaneethan, et al., Sens. Actuator. A -Phys. 269 (2018) 331–341.
[3] N.V. Toan, C.M. Hung, N.V. Duy, et al., Mater. Sci. Eng. B 224 (2017) 163–170.
[4] S. Xu, K. Kan, Y. Yang, et al., J. Alloys Compd. 618 (2015) 240–247.
[5] Y.S. Xu, T.T. Ma, Y.Q. Zhao, et al., Sens. Actuator. B -Chem. 300 (2019) 127042.
[6] Y.S. Xu, T.T. Ma, L.L. Zheng, et al., Sens. Actuator. B -Chem. 284 (2019) 202–212.
[7] X.X. Chen, Y.B. Shen, P.F. Zhou, et al., Sens. Actuator. B -Chem. 280 (2019) 151–161.
[8] Q. Zhang, H. Zhang, M.K. Xu, et al., Chin. Chem. Lett. 29 (2018) 538–542.
[9] T.T. Li, Y.B. Shen, X.X. Zhong, et al., J. Alloys Compd. (2019) 152927.
[10] Y.B. Shen, T.T. Li, X.X. Zhong, et al., Vacuum 172 (2020) 109036.
[11] S.K. Zhao, Y.B. Shen, P.F. Zhou, et al., Ceram. Int. 44 (2018) 753–759.
[12] K. Shingange, Z.P. Tshabalala, O.M. Ntwaeaborwa, et al., J. Colloid Interface Sci. 479 (2016) 127–138.
[13] S.K. Zhao, Y.B. Shen, P.F. Zhou, et al., Sens. Actuator. B -Chem. 282 (2019) 917–922.
[14] Y.B. Shen, W. Wang, X.X. Chen, et al., J. Mater. Chem. A 4 (2016) 1345–1352.
[15] X. Wang, F. Chen, M. Yang, et al., Sens. Actuator. B -Chem. 289 (2019) 195–206.
[16] T. Zhao, Y. Ren, G.Y. Jia, et al., Chin. Chem. Lett. 30 (2019) 2032–2038.
[17] P.F. Zhou, Y.B. Shen, S.K. Zhao, et al., J. Alloys Compd. 789 (2019) 129–138.
[18] S. G. R, N. M, V.L. Patil, et al., Sens. Actuator. B -Chem. 255 (2018) 672–683.
[19] Y.L. Wang, J. Liu, X.B. Cui, et al., Sens. Actuator. B -Chem. 238 (2017) 473–481.
[20] X.L. Ke, G.D. Zhu, Y. Dai, et al., J. Electroanal. Chem. 817 (2018) 176–183.
[21] C.B. Zhai, M.M. Zhu, L.N. Jiang, et al., Appl. Surf. Sci. 463 (2019) 1078–1084.
[22] N.V. Hieu, V.V. Quang, N.D. Hoa, et al., Curr. Appl. Phys. 11 (2011) 657–661.
[23] Y. Zeng, Z. Lou, L.L. Wang, et al., Sens. Actuator. B -Chem. 156 (2011) 395–400.
[24] Z.P. Tshabalala, K. Shingange, F.R. Cummings, et al., J. Colloid Interface Sci. 504 (2017) 371–386.
[25] P.-G. Su, L.-Y. Yang, Sens. Actuator. B-Chem. 223 (2016) 202–208.
[26] D.D. Trung, N.D. Cuong, K.Q. Trung, et al., J. Alloys Compd. 735 (2018) 787–794.
[27] F.J. Pan, H. Lin, H.Z. Zhai, et al., Sens. Actuator. B -Chem. 261 (2018) 451–459.
[28] Y.B. Shen, H.S. Bi, T.T. Li, et al., Appl. Surf. Sci. 434 (2018) 922–929.